THE JOURNAL OF BIOLOGICAL CHEMISTRY VOL. 287, NO. 32, pp. 26932–26943, August 3, 2012
© 2012 by The American Society for Biochemistry and Molecular Biology, Inc. Published in the U.S.A.

Role of the Iron Axial Ligands of Heme Carrier HasA in Heme Uptake and Release*[S]

Received for publication, March 26, 2012, and in revised form, June 14, 2012 Published, JBC Papers in Press, June 14, 2012, DOI 10.1074/jbc.M112.366385

Célia Caillet-Saguy[‡1], Mario Piccioli[§], Paola Turano[§], Gudrun Lukat-Rodgers[¶], Nicolas Wolff[‡], Kenton R. Rodgers[¶], Nadia Izadi-Pruneyre[‡], Muriel Delepierre[‡], and Anne Lecroisey[‡]

From the [‡]Unité de RMN des Biomolecules (CNRS URA 2185), Institut Pasteur, 28 Rue du Docteur Roux, 75015 Paris, France, [§]Center of Nuclear Magnetic Resonance and Department of Chemistry, University of Florence, Sesto Fiorentino, 50019 Florence, Italy, and the [¶]Department of Chemistry and Biochemistry, North Dakota State University, Fargo, North Dakota 58108-6050

Background: In the bacterial heme carrier HasA, an open to closed transition occurs with heme binding.
Results: Axial heme ligand mutants H32A and Y75A are both in a closed conformation.
Conclusion: Simultaneous binding of both axial heme ligands is not required for the closure of loop L1 in HasA.
Significance: The H32A mutant of HasA mimics a proposed structure involved in heme transfer to its partner HasR.

The hemophore protein HasA from *Serratia marcescens* cycles between two states as follows: the heme-bound holoprotein, which functions as a carrier of the metal cofactor toward the membrane receptor HasR, and the heme-free apoprotein fishing for new porphyrin to be taken up after the heme has been delivered to HasR. Holo- and apo-forms differ for the conformation of the two loops L1 and L2, which provide the axial ligands of the iron through His^{32} and Tyr^{75}, respectively. In the apo-form, loop L1 protrudes toward the solvent far away from loop L2; in the holoprotein, closing of the loops on the heme occurs upon establishment of the two axial coordination bonds. We have established that the two variants obtained via single point mutations of either axial ligand (namely H32A and Y75A) are both in the closed conformation. The presence of the heme and one out of two axial ligands is sufficient to establish a link between L1 and L2, thanks to the presence of coordinating solvent molecules. The latter are stabilized in the iron coordination environment by H-bond interactions with surrounding protein residues. The presence of such a water molecule in both variants is revealed here through a set of different spectroscopic techniques. Previous studies had shown that heme release and uptake processes occur via intermediate states characterized by a Tyr^{75}-iron-bound form with open conformation of loop L1. Here, we demonstrate that these states do not naturally occur in the free protein but can only be driven by the interaction with the partner proteins.

Iron is an essential nutrient for commensal and pathogenic bacteria. However, as the ferrous form is highly toxic for cells and the ferric form is scarcely soluble, it is usually sequestered in mammals by proteins such as ferritin, lactoferrin, and transferrin. Iron acquisition represents a challenge for bacteria invading mammalian hosts. Therefore, bacteria have developed different systems to acquire iron from all sources present in their hosts, including heme, either free or bound to hemoproteins. Among them, the heme uptake system Has has been identified in numerous pathogenic Gram-negative bacteria such as *Serratia marcescens* (1, 2), *Pseudomonas aeruginosa* (3), *Pseudomonas fluorescens* (4), *Yersinia enterolitica* and *Yersinia pestis* (5), and *Yersinia pseudotuberculosis* and *Erwinia carotorova*. Under iron deficiency conditions, these bacteria secrete small soluble heme carrier proteins, the hemophores. In the extracellular medium, hemophores either bind free heme or extract heme from host hemoproteins. Heme is then transported to the bacterial membrane for uptake through a specific receptor, HasR, and subsequent internalization. The hemophore HasA from *S. marcescens* (19 kDa) was the first to be discovered (1) and characterized (6). Structures of the wild type heme-loaded HasA (holo-$HasA_{WT}$) (Fig. 1) (7, 8) and heme-free HasA (apo-$HasA_{WT}$) (9) are available. The protein presents an original α/β fold with a highly curved seven-stranded antiparallel β-sheet on one face and a bundle of four α-helices on the other face. The heme binding pocket is mainly composed of two extended loops, L1 (Gly^{28}–Gly^{43}) and L2 (Tyr^{75}–Thr^{84}) that connect the α and β faces of the molecule. In holo-$HasA_{WT}$, the pocket assumes a closed conformation, with the two loops holding the heme through an uncommon pair of axial ligands as follows: a histidine (His^{32}) on loop L1 and a tyrosine (Tyr^{75}) on loop L2. In apo-$HasA_{WT}$ the loop L2 adopts a similar conformation as in holo-$HasA_{WT}$, whereas the loop L1 is displaced by about 30 Å and protrudes toward the exterior of the protein. The heme binding pocket thus adopts an open conformation in the apo-form.

The heme iron is in the ferric state and presents a thermal high spin (HS)[2]-low spin (LS) equilibrium, with the two species in fast exchange on the chemical shift NMR time scale (10). The affinity of $HasA_{WT}$ for heme is high ($K_a = 5.3 \times 10^{10}\ M^{-1}$), but

* This work was supported, in whole or in part, by National Institutes of Health Grants GM094039 (to G. S. L. R.) and AI072719 (to K. R. R.).
[S] This article contains supplemental Figs. S1–S6 and Tables S1–S3.
[1] Recipient of a Bourse Roux postdoctoral fellowship from Pasteur Institute. To whom correspondence should be addressed. Tel.: 33-140613667. Fax: 33-145688929; E-mail: ccaillet@pasteur.fr.

[2] The abbreviations used are: HS, high spin; LS, low spin; HSQC, heteronuclear single quantum coherence; HMBC, heteronuclear multiple bond correlation; GaPPIX, gallium(III) protoporphyrin IX; NMRD, nuclear magnetic resonance dispersion; rR, resonance Raman; Ches, *N*-cyclohexyl-2-aminoethanesulfonic acid; Tricine, *N*-[2-hydroxy-1,1-bis(hydroxymethyl)ethyl]glycine; 6cHS, six-coordinate H; 6cLS, six-coordinate LS; T, tesla.

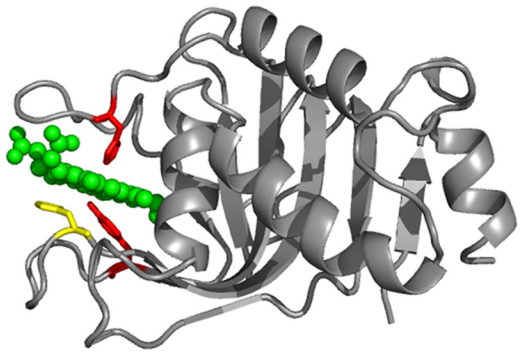

FIGURE 1. ***Ribbon* representation of the holo-HasA$_{WT}$ structure (Protein Data Bank code 1B2V).** The heme is in *green*. The two axial ligands, His^{32} and Tyr^{75}, are in *red*, and residue His^{83}, which is H-bonded to Tyr^{75}, is in *yellow*.

the two axial ligands make uneven contributions to heme binding. Indeed, whereas the H32A mutation results in a 5-fold decrease in affinity ($K_a = 1.0 \times 10^{10}$ M^{-1}), the Y75A mutation induces a 400-fold decrease ($K_a = 1.3 \times 10^{8}$ M^{-1}) (11). Coordination of the Tyr^{75} ligand is stabilized via a hydrogen bond between its Oη and the Nδ1 of the nearby histidine His^{83} (12, 13). Removal of His^{83} causes detachment of the Tyr^{75} ligand, thus giving rise to a series of pH-dependent equilibria among species with different axial ligation (13); in H83A at physiological pH, a five-coordinated HS species is observed. To decipher the role of His^{32} and Tyr^{75} in heme uptake and release processes, we have characterized the electronic properties and the iron coordination sphere of the holo-H32A and holo-Y75A mutants by means of NMR, nuclear magnetic resonance dispersion (NMRD), EPR, resonance Raman (rR), and UV-visible spectroscopies. The resulting picture is that the loss of Tyr^{75} produces species where the His^{32} imidazole ring is invariably bound to the heme iron whereas either His^{83} or H_2O bind on the side of the L2 loop, depending on pH. The loss of His^{32} gives rise, at physiological pH, to Tyr/H_2O axial ligation with $S = 3/2$ spin state. Interestingly, the lack of an amino acid binding in axial position on the L1 loop side does not induce the opening of the loop. These data are discussed in terms of heme uptake and release mechanisms.

EXPERIMENTAL PROCEDURES

Expression and Purification of the H32A and Y75A HasA$_{SM}$ Mutant Proteins—H32A and Y75A were constructed by *in vitro* site-directed mutagenesis as described previously (13). Proteins were obtained from the culture supernatants of *Escherichia coli* strain Pop3 (pSYC34PAM) grown at 30 °C in M9 minimal medium and purified as reported previously (6). Uniformly labeled ^{15}N and $^{15}N/^{13}C$ proteins were produced at 30 °C in M9 minimal medium containing $^{15}NH_4Cl$ and [^{13}C]glycerol as sole nitrogen and carbon sources. Purity of the proteins was checked by SDS-PAGE. The protein concentrations were determined using the $\epsilon_{277\,nm}$ values of 21,700 M^{-1} cm^{-1} for H32A mutant and 18,500 M^{-1} cm^{-1} for Y75A mutant (14). When necessary, the last C-terminal residues of the HasA proteins were cleaved by the *S. marcescens* protease Prt$_{SM}$ (15).

NMR Sample Preparation—Bovine hemin or gallium(III) protoporphyrin IX (GaPPIX) was dissolved in a minimal amount of 0.1 N sodium hydroxide (NaOH), centrifuged, and diluted with 20 mM sodium phosphate buffer, pH 7. Concentration of the hemin and GaPPIX solutions were measured in 0.1 M NaOH and in DMSO, respectively, using the $\epsilon_{385\,nm}$ NaOH and $\epsilon_{413\,nm}$ DMSO values of 58,440 M^{-1} cm^{-1} (16) and 249,000 M^{-1} cm^{-1}.[3] Freshly prepared hemin or GaPPIX solutions were added to the proteins in an ~1.2:1 ratio. The excess of hemin or GaPPIX was eliminated by gel filtration in 20 mM phosphate buffer at pH 7.0 to obtain 100% loaded proteins. The cyano-complexes were prepared by adding a 15 M excess of potassium cyanide (KCN) to the proteins (0.100 M KCN stock solution in 20 mM phosphate adjusted to the requested pH).

UV-visible Absorbance Spectroscopy—Protein samples for spectrophotometric pH titrations (pH 5.0–10.4) were prepared in a mixture of buffers (20 mM Mes, 20 mM Tris, and 20 mM Ches). The titrations were performed by adjusting pH with dilute hydrogen chloride (HCl) or NaOH solutions and monitoring the UV-visible spectrum. Dilution of each sample over the course of the titration was less than 2%. Twenty two spectra were recorded over the pH range of interest.

Resonance Raman Spectroscopy—Room temperature rR spectra were recorded from 25 to 80 μM protein samples in 5-mm NMR tubes spinning at ~20 Hz. The spectra were obtained with either 413.1 or 514.1 nm excitation from krypton and argon lasers, respectively, using the 135° backscattering geometry. Laser power at the samples ranged from 15 to 20 milliwatts. Sample integrity was checked by UV-visible absorbance spectroscopy before and after the rR spectra were recorded. The spectrometer was calibrated using the Raman bands of toluene, methylene bromide, and *N,N*-Dimethylformamide as external frequency standards.

The rR samples of H32A and Y75A examined for isotopic sensitivity were prepared by 30-fold dilution of stock protein solutions (2.0 mM Y75A and 1.3 mM H32A, respectively) into 50 mM *N*-cyclohexyl-3-aminopropanesulfonic acid buffer at pH 10.0, which had been prepared in $H_2{}^{18}O$ (96 atom % ^{18}O).

NMR Spectroscopy—NMR experiments were performed on protein samples ranging from 0.6 to 2 mM concentration in 20 mM phosphate buffer adjusted to the desired pH by adding dilute HCl or NaOH solutions. Unless otherwise specified, NMR spectra were recorded at 303 K. One-dimensional ^1H NMR spectra tailored to detect fast relaxing signals were acquired at 500 MHz (11.7 T) with a spectral width of 200 ppm and 8 K data points. Water suppression was achieved by fast repetition rate and presaturation during a 30-ms recycle delay. One-dimensional ^{15}N NMR spectra were acquired at 40 MHz (9.4 T) using a 450-ppm spectral width, 2 K data points, and a 10-ms recycle delay. One-dimensional ^{13}C NMR spectra were acquired at 175 MHz (14.4 T) with a spectral width of 500 ppm and 4 K data points. A triple resonance probe tailored for direct detection of ^{13}C signals was used throughout all ^{13}C NMR experiments. Experiments were performed with the ^{13}C-carrier frequency at −200, 150, 567, and 850 ppm to detect signals over wide spectral regions, using 10 or 200 ms as recycle delays. Several series of inversion recovery experiments were performed with the ^{13}C-carrier frequency at different positions to

[3] V. Kumar and I. Stojiljkovic, personnal communication.

properly invert and excite all ^{13}C resonances and determine their T_1 values. Recycle delays were 10 and 100 ms.

Chemical Shift Mapping—To express chemical shift changes of the individual amide groups, the chemical shift change (in ppm) was defined as shown in Equation 1 (17, 18),

$$\Delta\delta_{tot} = ((\Delta\delta HN)^2 + (0.16\Delta\delta N)^2)^{1/2} \quad \text{(Eq. 1)}$$

where $\Delta\delta H_N/N$ are the chemical shift differences of the corresponding amide $^1H/^{15}N$ nuclei between two protein forms, and 0.16 was the weighting factor for ^{15}N.

EPR Spectroscopy—EPR spectra were recorded with a Bruker ESP300E spectrometer fitted to an Oxford Instrument ESR900 helium flow cryostat. Experiments were carried out on protein samples with concentrations ranging from 0.1 to 0.5 mM in 50 mM sodium acetate buffer, pH 5.5, 50 mM phosphate buffer, pH 7.0, and 50 mM Tricine, pH 9.0. For spin intensity measurements of the low spin heme signal, EPR spectra were taken at 15 K in nonsaturating conditions, doubly integrated, and compared with a copper(II) sulfate standard of known concentration. Spin intensity measurements of the high spin heme signals were performed by comparing the double integration of the low field part of the signal to that given by a myoglobin sample of known concentration (19). When necessary, the deviation of the temperature dependence from the Curie's law was taken into account for high spin signals.

Magnetic Susceptibility Measurements—The magnetic susceptibility of WT and H32A HasA was measured by the modified Evans method (20–21) as reported previously (22). Coaxial NMR tubes were used with 1,4-dioxane as internal reference. The two protein samples had exactly the same concentration, *i.e.* 0.67 mM in 20 mM phosphate buffer, pH 5.7. The inner capillary contained the paramagnetic protein solution, and the outer tube contained the buffer solution only. The shifts of the proton signals of the reference molecule were measured on a Bruker AVANCE 800 spectrometer, operating at 18.7 T, over the 283–308 K temperature range. The inner-outer tube peak separation ($\Delta\delta$, expressed in ppm) for the standard molecule was measured and was attributed to the bulk susceptibility shift. The paramagnetic contribution to the molar susceptibility of the solute (χ_M^{PARA}) was related to the bulk susceptibility shift $\Delta\delta$ as indicated in Equation 2,

$$\Delta\delta = C_M\chi_M^{PARA}/3 \quad \text{(Eq. 2)}$$

in which C_M is the millimolar concentration of the protein, and χ_M^{PARA} is given in $m^3\ mol^{-1}$. The magnetic moment in solution (μ_{eff}) was then calculated according to Equation 3,

$$\mu_{eff}^2 = \chi_M^{PARA}\, 3kT/N_A\mu_0 \quad \text{(Eq. 3)}$$

where k is the Boltzman constant; T is absolute temperature; N_A is Avogadro's constant, and μ_0 is the vacuum permeability.

NMRD Measurements—Longitudinal water proton relaxation rates were measured with a prototype of a Stelar fast field cycling relaxometer (0.01–40 MHz proton Larmor frequency range) (23). The instrument provides R_1 values with an error smaller than 1%. ^1H NMRD profiles were obtained by plotting proton relaxation rates as a function of applied magnetic field. Reported profiles were obtained for WT and H32A samples that had exactly the same concentration (0.67 mM) in 20 mM phosphate buffer, pH 5.7.

RESULTS

Y75A Mutant

Global Fold—To probe the effect on the protein structure of replacing Tyr^{75} with the noncoordinating amino acid alanine, the ^1H-^{15}N heteronuclear single quantum coherence (HSQC) spectrum of the diamagnetic GaPPIX adduct of Y75A was compared with that of GaPPIX-$HasA_{WT}$, which is known to share the same structural features and the same axial ligand pair with the native paramagnetic iron(III) complex (24).

The ^1H-^{15}N HSQC spectra of GaPPIX-Y75A and GaPPIX-$HasA_{WT}$ recorded at pH 5.6 are essentially superimposable as shown in Fig. 2*A*. As expected, the signal of Tyr^{75} was missing in GaPPX-Y75A. Also the signal of Leu^{77} disappeared from the position observed in GaPPIX-$HasA_{WT}$; indeed, the HN of this residue in the wild type protein had a peculiar ^1H chemical shift (3.3 ppm) due to ring current effects from the nearby Tyr^{75} ring, and substitution of Tyr^{75} with an alanine removed the origin of its upfield shift. Small but significant chemical shift variations were observed for the remaining residues of loop L2, including His^{83}, and for the amino acids belonging to the region facing loop L2, such as 87, 128, 131, and 132. The chemical shift of His^{32} and of its surrounding residues was only slightly affected by the mutation, indicating that loop L1 did not change its conformation. The spectrum of GaPPIX-Y75A did not vary substantially at increasing pH values up to 8.2.

In summary, comparison of the GaPPIX-Y75A and GaPPIX-$HasA_{WT}$ spectra indicated that both proteins shared a very similar backbone conformation, including the two axial ligand bearing loops, independently of the pH. This result indicated that the heme-binding pocket of GaPPIX-Y75A maintained the same closed conformation as its WT counterpart. Accordingly, much larger differences were observed between the ^1H-^{15}N HSQC spectra of GaPPIX-Y75A and apo-$HasA_{WT}$, the latter providing the fingerprint for the open conformation of the hemophore (Fig. 2*B*).

Chemical shift differences between the ^1H-^{15}N HSQC spectra of the paramagnetic heme-loaded holo-Y75A and holo-HasA (supplemental Fig. S1) reflect, in principle, both conformational differences between the two proteins and variations in the hyperfine shift contribution arising from the different coordination state of the iron. However, given the results obtained for the gallium derivatives, the former effect was expected to be very minor. However, substitution of the axial Tyr^{75} ligand with a nonbonding alanine surely affected the electronic structure of the iron(III) center. Significant chemical shift changes were observed for the signals of Gly^{35}, Asn^{36}, Asn^{79}, and Ala^{82}, which were located in well resolved regions of the spectrum of holo-$HasA_{WT}$. Furthermore, in holo-Y75A, splitting was observed for most of the signals in the surrounding of the heme. This indicated that two different protein forms, in slow exchange on the chemical shift NMR time scale, exist for the mutant most probably due to two different sets of heme axial ligands. Upon increasing pH, the relative intensity of the two forms changes (supplemental Fig. S1). A pH-dependent transition between

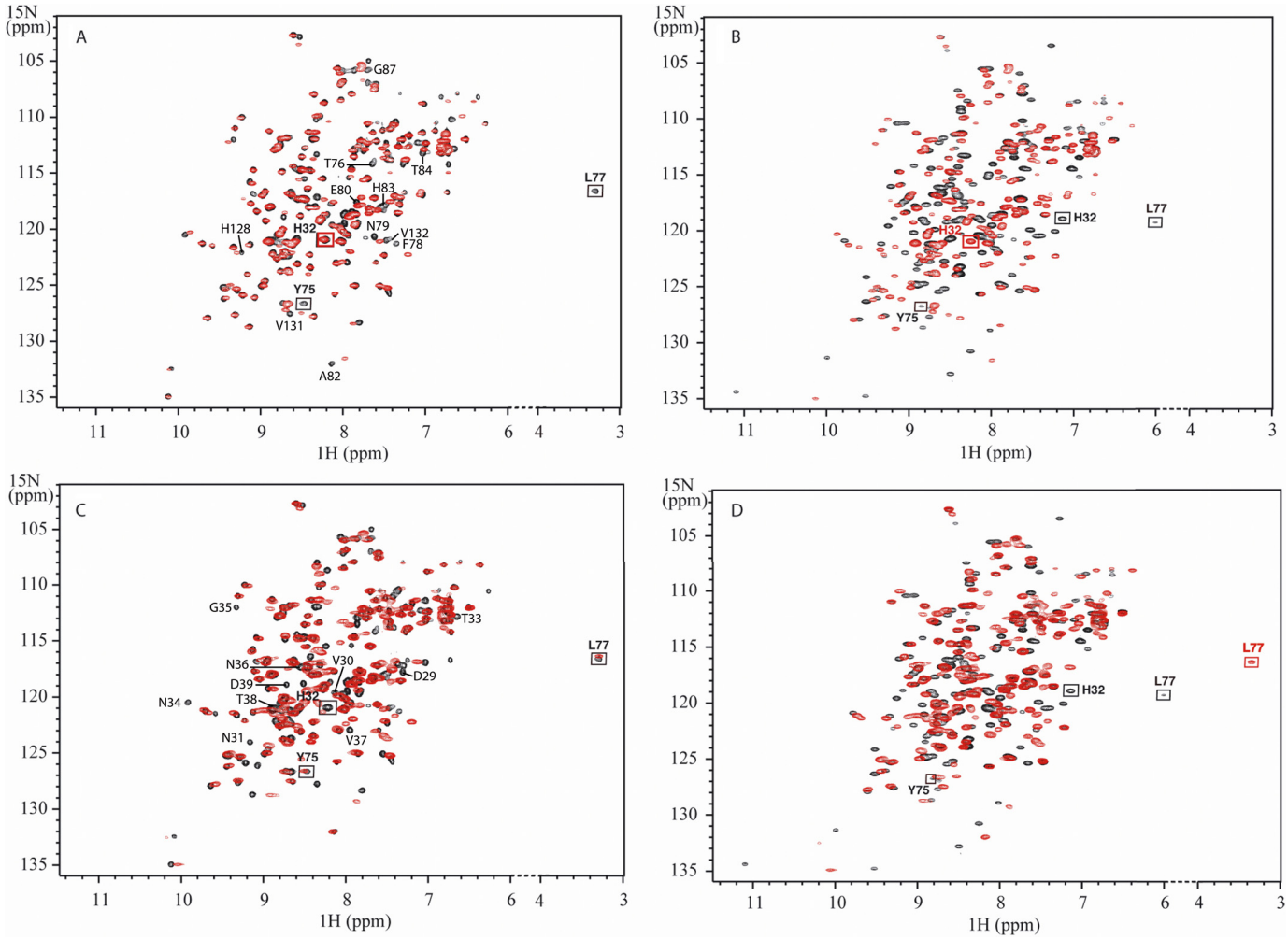

FIGURE 2. **Superimposition of ^{15}N-^{1}H HSQC spectra.** *A,* GaPPIX-Y75A (*red*) *versus* GaPPIX-HasA$_{WT}$ (*black*). ^{15}N-^{1}H correlations of residues of loop L2 and residues 87, 128, 131, and 132 of GaPPIX-HasA$_{WT}$ are indicated. *B,* GaPPIX-Y75A (*red*) *versus* apo-HasA$_{WT}$ (*black*). *C,* GaPPIX-H32A (*red*) *versus* GaPPIX-HasA$_{WT}$ (*black*). ^{15}N-^{1}H correlations of residues localized in the central part of the L1 loop, from Asp^{29} to Asp^{39}, of GaPPIX-HasA$_{WT}$ are indicated. *D,* GaPPIX-H32A (*red*) *versus* apo-HasA$_{WT}$ (*black*). Spectra were recorded at 303 K, at pH 5.6 in 20 mM sodium phosphate buffer.

protein forms with different heme iron coordinations was also observed by other spectroscopies, as detailed below.

Heme Iron Spin State and Coordination Sphere—The UV-visible spectrum of holo-Y75A shows meaningful changes over the 5.2–10.4 pH range (Fig. 3*A*). At pH 5.2, the presence of two Q bands at 533 and 564 nm, typical of LS ferric heme, together with a Q band at 497 nm and a charge transfer band at 629 nm, characteristics for HS ferric heme, was diagnostic for a mixture of the two spin states. The B band was observed at 406 nm. The HS species, predominant at acidic pH, was converted to an LS species with increasing pH values as reported by the B band shifting to 410 nm and the charge transfer (CT) band losing intensity. Determination of pK_a values using the absorbance values at a single wavelength is shown in Fig. 3*A, inset.* Wavelength data for 406 and 629 nm yield a pK_a value of 7.2 ± 0.2 for the HS → LS transition. Fitting the intensity of the band at 533 nm data gave a pK_a value of <6, which suggested the presence of a further low spin species, as detected by rR (see below).

The pH dependence of the spin states of holo-Y75A was also observed by rR spectroscopy. The high frequency rR spectra at pH 5.2 revealed bands at 1477 cm^{-1} (ν_3) and 1557 cm^{-1} (ν_2) that are characteristic of a six-coordinate HS (6cHS) state, together with three bands at 1502 (ν_3), 1576 (ν_2), and 1633 cm^{-1} (ν_{10}), typical of a six-coordinated LS (6cLS$_1$) state (Fig. 3*B*). Upon raising the pH from 5.2 to 6, the intensity of the 6cHS ν_3 and ν_2 bands decreases significantly while that of the 6cLS ν_3 band increases. Moreover, the 6cLS$_1$ ν_2 band at 1576 cm^{-1} shifted to 1579 cm^{-1}, and a second 6cLS ν_{10} band became observable at 1640 cm^{-1}, consistent with the presence of a second six coordinate LS (6cLS$_2$) species. The LS$_2$ species became predominant at high pH. The low frequency spectrum of holo-Y75A also reflects this pH dependence (Fig. 3*C*). The most notable changes occurred between pH 5.2 and 6.0 in the vinyl and propionate group bending frequencies. One of the vinyl bending bands $\delta(C_\beta C_a C_b)$ shifted from 421 to 427 cm^{-1}, and the propionate bending band $\delta(C_\beta C_c C_d)$ at 380 cm^{-1} shifted to 378 cm^{-1}, thus indicating changes in the environment of the peripheral heme substituents. Comparison of the peripheral group bending frequencies for alkaline Y75A with those of HasWT (13) (supplemental Fig. S2) indicated that the vinyl and propionates groups have different environments in these proteins with the frequencies of the $\delta(C_\beta C_c C_d)$ band for Y75A suggesting a weaker hydrogen bonding environment for at least one propionate group relative to that in HasAWT. The possi-

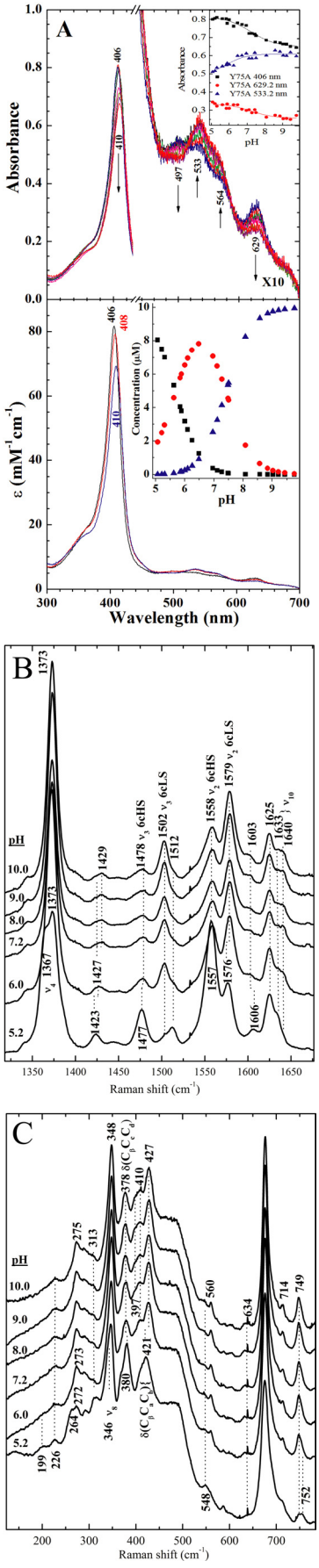

bility of a 6cLS hydroxide complex at alkaline pH was considered by examining Y75A at pH 10.0 in $H_2{}^{18}O$. Heme hydroxides typically exhibit Raman bands between 440 and 560 cm^{-1}. As these bands correspond to normal modes that are dominated by Fe-OH stretching, their frequencies are sensitive to changes in the reduced mass of the FeOH oscillator and shift ~20 cm^{-1} to lower frequency in $H_2{}^{18}O$ (25 and references therein). No isotope shift was observed suggesting that the $6cLS_2$ complex was not a hydroxide complex.

The EPR spectrum of Y75A at pH 5.5 indicated the presence of an HS ($g_\perp = 5.76$ and $g_\parallel = 2.2$) and an LS ($g = 2.87$, 2.28, and 1.54) species. The signal of the HS form decreased with increasing pH up to 9.5, whereas that of the LS species increased (data not shown).

One-dimensional ^1H NMR spectra of holo-Y75A, recorded from pH 4.6 to pH 9.9, show two sets of signals in a 80:20 ratio corresponding to the two possible orientations of the heme along the α-γ meso axis, as already observed for holo-$HasA_{WT}$ and holo-H83A mutant (10, 13). Hereafter, only the major set will be considered; however, the observed behavior also holds for the minor set of resonances. The spectrum at pH 5.6 (Fig. 4*A*) displays two groups of resonances, in agreement with the HSQC results. The first one (form A) was characterized by broad peaks, in the 80 to 40 ppm range. The second (form B) has sharper peaks, in the range 40 to 15 ppm. Upon increasing pH, form A decreases in intensity to the benefit of form B (Fig. 4*B*). The chemical shift values of the B form showed a slight pH dependence at pH < 6, consistent with the LS_1-LS_2 equilibrium detected by visible and rR spectroscopies (data not shown). The four most intense signals of form A (57.5, 52.8, 50.1, and 44.6 ppm at pH 5.6 and 303 K) were attributable to the four heme methyls. Their average chemical shift, 51.2 ppm, was intermediate between those expected for purely HS (S = 5/2) and purely LS (S = 1/2) heme iron(III). Line widths of the order of 350 Hz and short T_1 values (4–5 ms) of methyl resonances were comparable with those of $HasA_{WT}$, which experienced a thermal HS/LS equilibrium, fast on the NMR chemical shift time scale. A broad signal, exchangeable in deuterium oxide (D_2O), occurred at 73.6 ppm with linewidth of about 1500 Hz and a T_1 value shorter than 1 ms. By analogy with the wild type case, it can be attributed to the HNδ1 of the heme-bound His^{32}. The temperature dependence of His^{32} HNδ1 chemical shift and heme methyl resonances showed a nonlinear behavior indicating a non-pure spin state (supplemental Fig. S3). This is, again, in analogy with previous observations on holo-$HasA_{WT}$. To further characterize the A form, a one-dimensional ^{13}C spectrum was recorded at pH 5.6, showing three major and three minor hyperfine shifted signals, respectively labeled *B*, *C*, *F* and

FIGURE 3. **Holo-Y75A UV-visible and resonance Raman spectra, at pH ranging from 5.1 to 10.** *A, top panel,* UV-visible spectra. *Arrows* indicate the direction of the absorbance change as the pH is increased. The *inset* shows all data points at the indicated wavelengths and titration curves calculated by global nonlinear least squares analysis. *Bottom panel,* component spectra obtained from a global fit of all 22 pH titration spectra of holo-Y75A. The *black line* is the acidic component; the *red line* is the intermediate pH component; the *blue line* is the alkaline species. *Inset,* species distribution as a function of pH obtained from the global fit. ■, the acidic component; ●, the intermediate pH component; ▲, the alkaline species. *B,* Soret-excited high frequency; *C,* low frequency rR spectra at the indicated pH values.

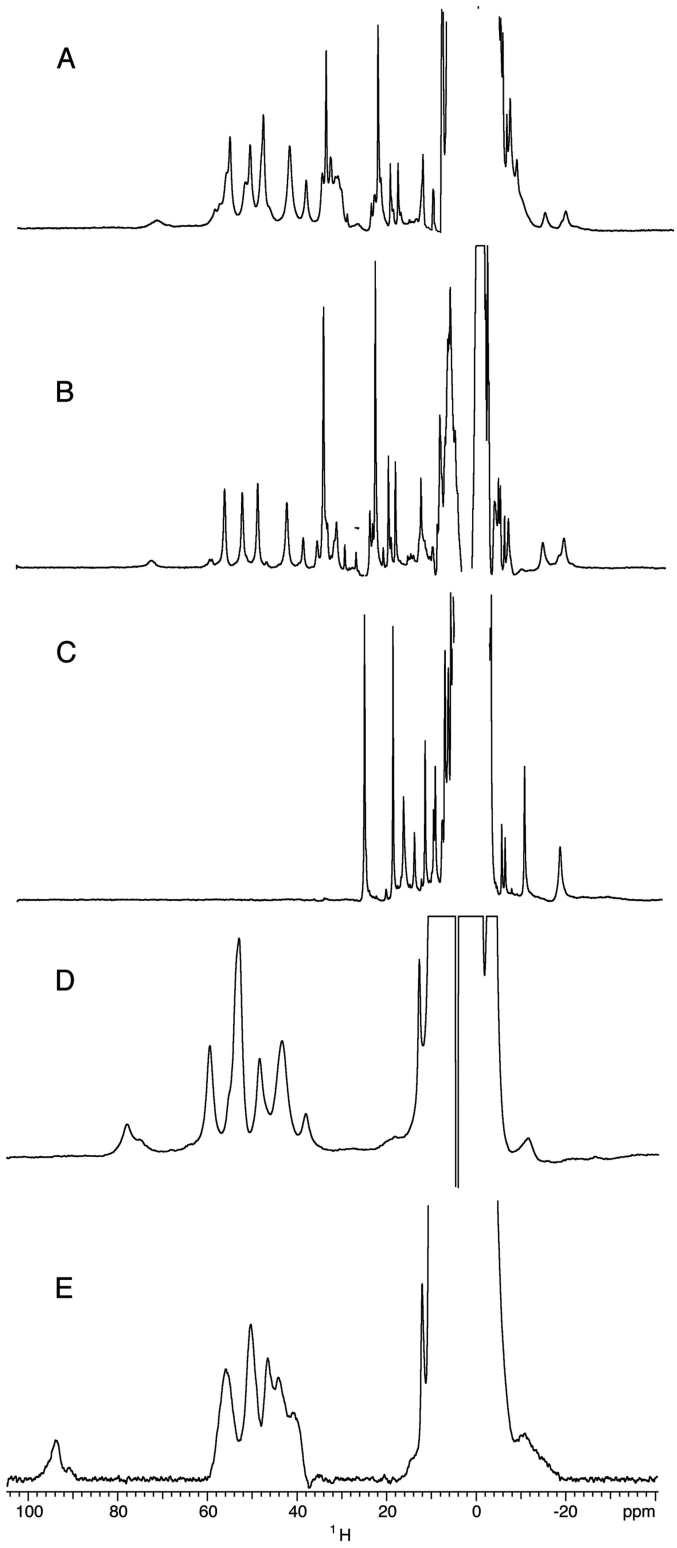

FIGURE 4. **^{1}H NMR spectra.** *A,* holo-Y75A at pH 5.6; *B,* holo-Y75A at pH 8.2. *C,* holo-Y75A cyanide adduct at pH 7.3; *D,* holo-H32A at pH 5.6; *E,* holo-H32A at pH 9.1. Spectra were recorded at 303 K, in 20 mM phosphate buffer.

A, D, E in the 210–670 ppm region (Fig. 5*A*), with line widths in the range 800–3000 Hz and T_1 values shorter than 1 ms (supplemental Table S1). Analogous signals in the WT and H83A proteins were previously attributed to His^{32} imidazole ring resonances (Fig. 5*B*) (13). Their shift increases at increasing temperatures. Insights on the axial ligation in Y75A could be gained by comparing the coordination sphere of the previously characterized protein forms and their observed chemical shifts. Average chemical shift values for ^{13}C resonances of His^{32} and ^{1}H resonances of heme methyls and His^{32} H Nδ1 measured for holo-HasA$_{WT}$, holo-H83A, and for the A form of holo-Y75A are reported in Table 1. The pure five-coordinate HS (5cHS) species in holo-H83A, where His^{32} is the only axial ligand, had the highest chemical shifts. Species with His^{32} and a sixth ligand (Tyr^{75} in holo-HasA$_{WT}$ and $H_2O^{\delta-}$ in holo-H83A) have somewhat lower shifts, which, with temperature, deviate from a purely Curie behavior. On these bases, and due to the lack of hyperfine shifted signals attributable to a second protein axial ligand, we propose that form A of holo-Y75A was an His^{32}-Fe-$H_2O^{\delta-}$ moiety. The preserved conformation for loop L2 upon removal of Tyr^{75} that emerges from the HSQC fingerprint was consistent with a stabilization of the interaction between the loop and the heme iron mediated by a water molecule that forms an H-bond, probably with His^{83}.

The B form of holo-Y75A included sharp ^{1}H signals for heme methyls (line width ≈150 Hz) with average chemical shift of 45.9 ppm and linear Curie temperature dependence (supplemental Fig. S3). All these NMR parameters suggest a pure LS species. Insight on the nature of the axial ligands of Y75A was further obtained from ^{15}N heteronuclear multiple bond correlation (HMBC) experiments tailored for the detection of imidazole resonances. ^{15}N HMBC spectra of GaPPIX-Y75A and GaPPIX-HasA$_{WT}$ (supplemental Fig. S4) were recorded from pH 5.4 to 9.1. Both GaPPIX-Y75A and GaPPIX-HasA$_{WT}$ spectra gave the same pattern of cross-peaks for His^{17}, His^{32}, His^{128}, and His^{133}, leading to their assignment and to the identification of His^{32} as an axial ligand in GaPPIX-Y75A (supplemental Table S2). However, two very close sets of cross-peaks corresponding to two different forms were observed for His^{32} resonances (largest chemical shift differences of 0.05 ppm in proton and 0.6 ppm in nitrogen). One set was predominant at acidic pH and corresponds to form A and the other at basic pH corresponds to form B. The Hϵ1 and Hδ2 protons were highly upfield shifted, and the cross-peak patterns indicate the formation of the Nδ1H tautomer. These data show that His^{32} was a ligand in both forms, coordinating the metal through its Nϵ2. Two sets of connectivities, corresponding to A and B forms, were also present for His^{83} in GaPPIX-Y75A spectra. The set dominant at pH 5.4 had a cross-peak pattern resembling that of His^{83} in GaPPX-HasA$_{WT}$ and was consistent with a protonated imidazole ring. The His^{83} signals of the B form indicate a neutral imidazole ring and the formation of the Nϵ_2H tautomer, with the Nδ1 nitrogen deprotonated and both Hϵ1 and Hδ2 protons further upfield shifted with respect to the A form. These data are consistent with the previous observation that, in holo-Y75A, His^{83} was a heme iron ligand and suggest an unusual coordination of His^{83} via its Nδ1 (12). Although bis-His coordination is commonly encountered in heme proteins, binding of His through Nδ1 is rare and occurs only in the presence of specific steric requirements (26). Here, we propose that His^{83} Nδ1 forms a hydrogen bond with the coordinated water molecule in form A. The binding of its Nδ1 to the heme iron in form B was easier than binding

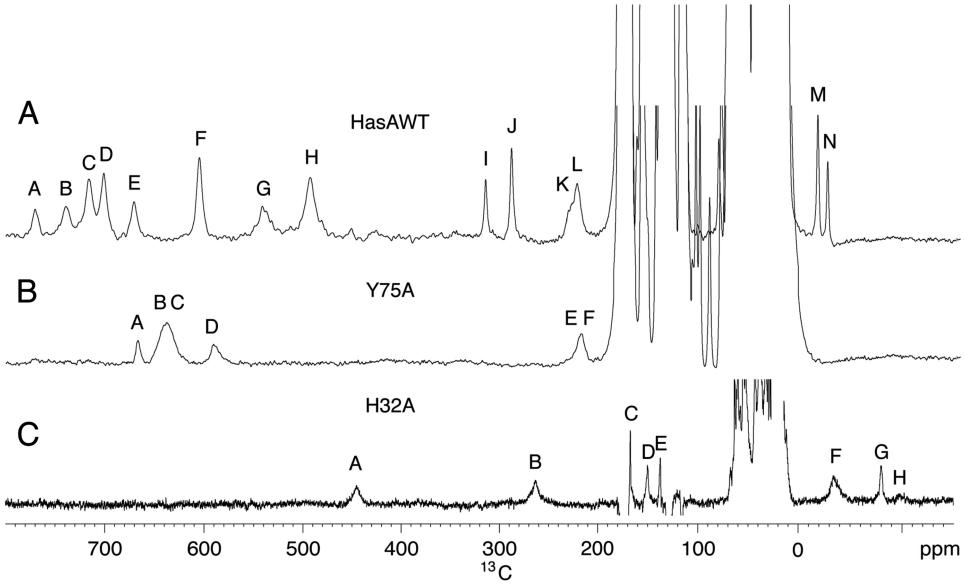

FIGURE 5. **^{13}C NMR spectra at pH 5.6.** *A,* 1.6 mM holo-HasA$_{WT}$ (taken from Ref. 10); *B,* 2.0 mM holo-Y75A; and *C,* 1.2 mM holo-H32A. Spectra were recorded at a 175 MHz ^{13}C Larmor frequency at 303 K in 20 mM phosphate buffer.

TABLE 1

Chemical shift fingerprint of the nature of the sixth heme iron ligand in HasA$_{WT}$ and its mutants

Diagnostic values are associated with the average heme-methyl ^{1}H chemical shift, chemical shift of HNδ1 of His^{32}, and ^{13}C average chemical shift for the hyperfine shifted resonances of His^{32}.

Protein	HasA$_{WT}$(10)	H83A (13)			Y75A (A form) (Ref. 10 and this work)	
Axial ligation	His^{32}-Fe-Tyr^{75}	His^{32}-Fe	His^{32}-Fe-H$_2$O$^{\delta-}$	His^{32}-Fe-OH$^-$	His^{32}-Fe-H$_2$O$^{\delta-}$	
^{1}H CH$_3$	40.0	71.3	54.0	35.2	51.2[a]	45.9[b]
His^{32} HNδ^1	66.3	103	ND[c]	ND	73.6	61
^{13}C H32	439.1	530.4	ND	ND	475.1	ND

[a] Data were at pH 5.6.
[b] Data were at pH 9.5.
[c] ND means not determined.

of His^{83} Nϵ2, which would necessitate a rotation of the imidazole ring.

Finally, addition of cyanide (CN^-) induces formation of a new protein form. The UV-visible spectrum of the cyanide adduct was independent over the 7.3–9.5 pH range and showed a B band at 416 nm and Q bands at 536 and 560 nm (data not shown). The ^{1}H NMR spectrum is shown in Fig. 4*C*. According to their intensities, the two signals at 27.1 and 20.8 ppm were attributable to heme methyl groups. It was clear that both the A and B forms of holo-Y75A converted to the same LS cyanide derivative, where His^{32} was one of the two axial ligands and CN^- the other. Cyanide binding in the sixth position did not occur in the H83A variant, thus indicating that His^{83} triggered the binding of cyanide in the distal cavity of the protein. Using the heuristic equation proposed by Bertini *et al.* (27) to calculate the hyperfine shifts of the heme methyls in the cyanide adduct of hemoproteins, the observed heme pattern fits with His^{32} maintaining the same orientation with respect to the heme plane as in the wild type protein.

H32A Mutant

Global Fold—As for Y75A, the gallium complex of H32A was used to study the effect of the substitution of the His^{32} axial ligand by a noncoordinating residue on the protein fold. The ^{1}H-^{15}N HSQC spectra of GaPPIX-H32A and GaPPIX-HasA$_{WT}$, recorded at pH 5.6 (Fig. 2*C*), are very similar (average chemical shift difference 0.06). The signals of the L2 loop residues, including Tyr^{75}, were essentially superimposable in the two spectra. As expected, chemical shift changes concern residues localized in the central part of the L1 loop, from Asp^{29} to Asp^{39} (average chemical shift difference of 0.16 ppm; supplemental Table S3), *i.e.* the L1 portion surrounding His^{32}. Smaller but meaningful shift changes were also observed for residues 56–65 on β3, β4, and the connecting loop, which face the portion of loop L1 containing His^{32}. Chemical shift differences observed between HSQC spectra of GaPPIX-H32A and apo-HasA$_{WT}$ were larger; chemical shift differences of >0.50 ppm were observed for the entire L1 loop and for the β3, β4, and connecting loop fragment. Differences up to 2.3 ppm were observed for residues 77, 78, and 83–85; these are residues on loop L2 in closest contact with the heme (Fig. 2*D* and supplemental Table S3). In summary, mutation of His^{32} did not alter the structure of the protein and did not trigger the opening of the L1 loop even though minor conformational changes likely occur in the central part of this loop. GaPPIX-H32A and consequently heme loaded H32A adopted a closed conformation. The HSQC spectrum of GaPPIX-H32A recorded at pH 9 was similar to the one recorded at pH 5.6 with only a small shift of some resonances (data not shown), thus indicating that the protein structure was not affected by pH.

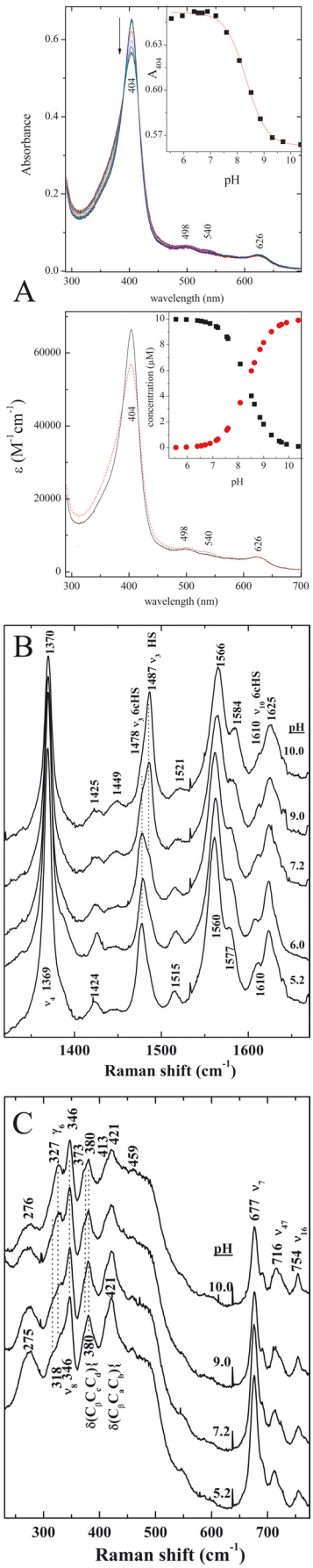

The comparison of the chemical shift patterns in the ^{1}H-^{15}N HSQC spectra of the paramagnetic heme-loaded H32A and $HasA_{WT}$ (supplemental Fig. S1) at acidic pH highlight some shift differences for residues in both L1 and L2 loops. Obviously, signals of Asp^{29}, Gly^{35}, Asn^{36}, Ala^{40}, Asn^{79}, and Ala^{82} changed their shift in holo-H32A, consistent with the slight conformational changes observed for the gallium adduct and with differences in the coordination state of the heme iron and therefore in its magnetic properties. As observed for the GaPPIX-H32A derivative, spectral differences in holo-H32A HSQC spectra between pH 5.6 and 9.1 were minor, indicating the same overall backbone conformation for the protein over the investigated pH range.

Heme Iron Spin State and Coordination Sphere—UV-visible spectra of H32A are shown in Fig. 6*A* as a function of pH. The B band at 404 nm, the Q bands at 498 and 540 nm, and a charge transfer band at 626 nm were observed at pH 5.2. The CT band at 626 nm persisted throughout the pH titration, suggesting that the heme was always HS. The *inset* in Fig. 6*A* shows the plot of 404 nm absorbance *versus* pH, which yields a pK_a of 8.3 ± 0.2. The component spectra obtained from the global fit were consistent with the interconversion of two HS species.

The rR spectra of ferric holo-H32A recorded over the pH range 5.2 to 10.0 were consistent with the pH-dependent interconversion of two HS species. In the high frequency spectra (Fig. 6*B*) at pH 5.2, the major component contains 6cHS heme with a ν_3 band at 1478 cm^{-1}, a ν_2 band at 1560 cm^{-1}, and a ν_{10} band at 1611 cm^{-1}. As the pH was raised, this ν_3 band loses intensity with the appearance of a new band at 1487 cm^{-1}. This frequency falls at the low end of the frequency range expected for 5cHS proteins (28). A similar frequency has been observed for the 5cHS form of holo-H83A mutant (13). The two HS species in equilibrium in holo-H32A were therefore six- and five-coordinated. In the spectra at pH 10, the intensities of the ν_3 and ν_4 bands were almost equal. This rR signature is characteristic of 5cHS hemes having an axial anionic ligand bound through an oxygen atom such as catalase, ShuT, and CcmE (29–31). These proteins, like some mutant hemoproteins with a tyrosinate as single axial ligand, have $I(\nu_4)/I(\nu_3)$ intensity ratios in the 1–1.5 range. Such intensity ratios have also been reported for 5cHS hemoproteins with a coordinated hydroxide ion (32, 33). No isotope shift was observed for H32A in $H_2{}^{18}O$ at pH 10.0 indicating that a hydroxide complex was not formed and that Tyr^{75} was the most likely anionic oxygen heme ligand.

Conversion from an acidic form to a basic form of holo-H32A was also observed in the low frequency rR spectra (Fig. 6*C*). Although the frequencies of the bands associated with the peripheral substituents (380 and 421 cm^{-1}) do not change,

FIGURE 6. **Holo-H32A UV-visible and resonance Raman spectra, at pH ranging from ~5.3 to 10.5.** *A, top panel,* UV-visible spectra (the *arrow* indicates the direction of the absorbance change as the pH is increased). *Inset,* Soret absorbance ($A_{404\ nm}$) *versus* pH; points are experimental absorbances, and the *solid line* is the titration curve calculated by global nonlinear least squares analysis. *Bottom panel,* component spectra obtained from a global fit of all 21 pH titration spectra of holo-H32A. The *black line* is the acidic component; the *dotted red line* is the alkaline species. *Inset,* species distribution as a function of pH obtained from the global fit. ■, the acidic component; ●, the alkaline species. *B,* high frequency; *C,* low frequency rR spectra (413.1 nm excited) at the indicated pH values.

TABLE 2

Bulk susceptibility shifts (Δδ, ppm) for H32A and WT HasA measured against 1,4-dioxane by the Evans method in the temperature range 283–308 K at pH 5.7 and 800 MHz

The resulting paramagnetic contribution to the molar susceptibility (χ_M^{PARA}, $m^3\ mol^{-1} \times 10^8$) and the effective magnetic moment (μ_{eff}, μ_B) of the paramagnetic center are also reported.

	H32A			WT		
T	Δδ	χ_M^{PARA}	μ_{eff}	Δδ	χ_M^{PARA}	μ_{eff}
K	*ppm*	*($m^3\ mol^{-1} \times 10^8$)*	μ_B	*ppm*	*($m^3\ mol^{-1} \times 10^8$)*	μ_B
283	19.9	8.91	3.86	11.7	5.23	3.02
288	19.3	8.64	3.88	12.4	5.56	3.11
293	19.0	8.51	3.88	12.9	5.78	3.20
298	18.6	8.33	3.87	13.6	6.09	3.31
303	18.2	8.15	3.86			
308	17.8	7.97	3.85	13.9	6.22	3.40

shoulders appear on both of these bands as the pH was increased suggesting that possibly the environment of at least one vinyl and one propionate group was altered. The most dramatic change was the appearance of a band at 327 cm^{-1}. This band is tentatively assigned to an out-of-plane mode γ_6 (pyrrole tilt) based on the frequency similarities with metMb (34), CCP (35), and TcAPII (36). Resonance enhancement of this mode was activated by doming of pentacoordinated hemes.

The EPR spectrum of holo-H32A recorded at 15 K in the pH range 5.5–9.5 was dominated by an HS species with $g_\perp = 5.75$ and $g_\parallel = 2.00$ (supplemental Fig. S5). The $g_\perp$ value of 5.75 was too low for a pure high spin state. Based on the pH-independent $g_\perp$ value of 5.75, the spin state is best described as a quantum spin admixture having 12% of an S = 3/2 iron spin state with unresolved g_1 and g_2 (37, 38).

^{1}H NMR one-dimensional spectra of holo-H32A were recorded from pH 4.5 to pH 10.3. As for holo-Y75A, two sets of signals due to different heme orientations were observed (70:30 ratio), and only the major one was considered hereafter. The spectrum at pH 5.6 and 303 K shows signals in the 35–60 ppm range, with line widths of about 900 Hz and T_1 values around 1–2 ms (Fig. 4*D*). Peaks at 59.4, 53.5, 52.8, and 48.3 ppm were attributable to the four heme methyls. Their observed chemical shifts and relaxation rates were smaller than those observed for other HS heme iron(III) hemoproteins. A signal, not exchangeable in D_2O even after a few months at 280 K or after heating the sample at 318K, accounted for a single proton, with a linewidth of about 1400 Hz and T_1 values smaller than 0.5 ms occurred at 77.8 ppm. An additional unexchangeable signal, detectable only upon increasing the temperature to 318 K, was observed at 84.1 ppm. Attribution of these two resonances to meta protons of the tyrosine ligand is consistent with previous literature data on catalase (39) and on the H93Y mutant of myoglobin (40). Increasing the pH results in a small shift of all resonances (Fig. 4*E*), less than 6 ppm over the studied pH range (except for the signal resonating at 77.8 ppm at pH 5.6, which presents a shift of 19 ppm). This behavior was consistent with a rapid equilibrium on the NMR time scale between the two species that rR spectroscopy showed to be 6cHS and 5cHS. The low value of the heme methyl chemical shifts points, however, to a spin state that was lower than S = 5/2 heme.

To further investigate this aspect, Evans measurements were performed in the temperature range 283–308 K and pH 5.7. Table 2 reports the shifts together with the resulting average paramagnetic molar susceptibility and effective magnetic moment; those of the WT protein have been also measured for comparison purposes. The effective magnetic moment for H32A was of the order of ~3.87 μ_B. It was essentially invariant over the investigated temperature range and coincided with what was expected for an iron(III) S = 3/2 species (theoretical spin only value of 3.87 μ_B). At variance, the WT protein has a slightly lower and temperature-dependent μ_{eff}, with smaller values at low temperature (Table 2). The magnetic properties of holo-$HasA_{WT}$ were consistent with our previous proposal, based on the temperature dependence of NMR chemical shifts and the rR spectra, that the proteins undergo a spin-dependent equilibrium between a low spin S = 1/2 form (dominant at lower temperature and that would be characterized by μ_{eff} values in the 1.9–2.3 μ_B range due to the large orbital contribution characteristic of this spin state) and a high spin form (dominant at higher temperature and that would be characterized by a μ_{eff} of 5.9 μ_B). At room temperature, the measured μ_{eff} of 3.31 μ_B would account for relative populations of low spin and high spin states of ~70 and ~30%, respectively. Effective magnetic moments lower for WT than for H32A were consistent with ^{1}H average chemical shift for heme methyls, which was smaller for WT than for H32A (~40 ppm *versus* ~50 ppm). Structural determinants for the presence of S = 3/2 heme iron(III) have been discussed for other proteins (41). A decreased axial ligand field strength was typically accompanied by a strengthening of the equatorial field and destabilization of the d_{x2-y2} orbital, which facilitates attainment of the S = 3/2 electron configuration. This could be the case in H32A, where the axial bond with the strong His ligand was removed and possibly replaced by a water molecule (as it results from NMRD measurements, see below).

The bond with Tyr^{75} appears, instead, unaffected. ^{15}N HMBC experiments of GaPPIX-H32A recorded at pH ranging from 5.6 to 9 confirm the H-bonding of His^{83} with Tyr^{75}. GaPPIX-H32A spectra give the same pattern of cross-peaks as GaPPIX-$HasA_{WT}$, thus allowing the assignment of the histidines (supplemental Fig. S4). The pattern of His^{83} was consistent with a protonated imidazole ring over the pH range studied. The Hϵ1 and Hδ2 protons resonances are upfield shifted and similar to those of GaPPIX-$HasA_{WT}$ and of the A form of GaPPIX-Y75A (supplemental Table S2). The one-dimensional ^{13}C NMR spectrum of holo-H32A at pH 5.6 and 303 K (Fig. 5*C*) shows two broad and fast relaxing hyperfine-shifted signals in the downfield region at 444.2 ppm (*A*) and 263.2 ppm (*B*) and three in the upfield region at −34.2 ppm (*F*), −80.4 ppm (*G*), and −98.0 ppm (*H*). An inversion recovery sequence allowed us

to identify three additional signals with short T_1 and large line widths that were buried in the diamagnetic envelope at 167.4 ppm (*C*), 150.2 ppm (*D*), and 137.4 ppm (*E*), respectively. Signals A–H can be assigned to the axial ligand Tyr^{75}, in both A and B forms. All our data point to the fact that Tyr^{75} was bound to the metal ion as follows: (*a*) the number and the relaxation rates of hyperfine shifted signals observed in ^{13}C direct detection; (*b*) the occurrence of a tyrosinate as a fifth ligand of the heme suggested by rR; (*c*) the presence of a downfield shifted signal in ^{1}H NMR spectra analogous to that attributed to meta tyrosine protons in catalase and H93Y Mbl, and (*d*) the fact that His^{83} was hydrogen bonded to Tyr^{75} as shown by HMBC spectra. Lack of further hyperfine shifted signals in NMR spectra strongly support the idea that the second axial ligation position in H32A was either empty or occupied by a solvent molecule. This ambiguity has been removed thanks to the use of NMRD measurements. The WT protein has a coordination sphere containing only protein amino acids. Consistently, it has low water proton relaxation rates (supplemental Fig. S6) that correspond to the values expected for systems where only an outer sphere mechanism is operating (42). On the contrary, in H32A solution much faster water relaxation rates are measured (supplemental Fig. S6), which was consistent with the presence of a water molecule coordinated to the heme iron and in fast exchange with bulk solvent.

No spectral changes were observed upon addition of a 15-fold excess of buffered KCN to holo-H32A at pH 7.3 or pH 9.4 (data not shown). Thus, neither the 6c form dominant at neutral pH or the high pH 5c form bind cyanide. Reduced affinity of cyanide for 5c or 6c with a weak axial ligand iron(III) hemes has already been observed in systems in which cyanide binding was not stabilized by H-bonding interactions (43). In addition, the L1 loop site results were largely negative due to amino acid side chains and to the proximity of carboxylate groups from heme propionates, thus creating an electrostatic repulsion between this region of the protein and anionic ligands. Coordinating water in fast exchange with bulk solvent and the inability to bind cyanide are two features both pointing to unrestricted or only slightly restricted mobility of small molecules on the L1 site.

DISCUSSION

The structures of holo- and apo-HasA are largely different due to the conformation of the two loops L1 and L2 that in the holo-form provide the heme-iron(III) axial ligands. The apo-form has an "open" conformation where the two loops are completely disconnected one another. Upon heme uptake, establishment of coordination bonds between iron(III) and His^{32} Nϵ2 on loop L1 and Tyr^{75} Oη on loop L2 induces a large conformational rearrangement wherein the loops close onto the heme. Based on the overall shape of HasA in its apo- and holo-forms, the heme binding process has been described as resembling a "fish biting the heme" (7).

In the WT protein, the heme is linked to the L2 loop on one side via Tyr^{75}. The strength of this bond is modulated by the presence of an H-bond between His^{83} Nϵ2 and the Tyr^{75} Oη, which impart a certain degree of tyrosinate character to Tyr^{75}, thus increasing its coordinating ability. Still, the protein undergoes a thermal spin equilibrium between an S = 1/2 state corresponding to $His/Tyr^{\delta-}$ axial ligation and an S = 5/2 state where Tyr^{75} coordination is weakened (Scheme 1*A*). At room temperature, about 70% of the protein population is in the low spin configuration, as determined here by magnetic susceptibility measurements.

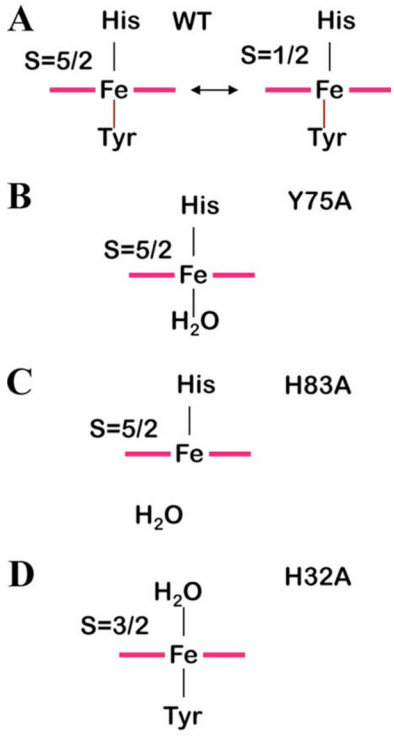

SCHEME 1. **Species present at physiological pH for $HasA_{WT}$ and mutants.**

The heme is interacting with loop L1 on the other side via the coordination bond between iron and His^{32} Nϵ2 and through an H-bond network that involves the solvent-exposed propionates and residues His^{32}, Asn^{34}, and Gly^{35}. The presence of the heme provides a link between L1 and L2. We have demonstrated here that such a link, responsible for the closed conformation of $HasA_{WT}$, is maintained in the protein variants where either axial ligand is replaced by an alanine.

Tyr is a relatively weak ligand for iron(III) (40, 44), and its presence is not vital for the protein fold. In the Y75A mutant loop L2 remains connected to L1 through the heme thanks to the presence of a water molecule (or of His^{83} at high pH) in place of Tyr^{75}, as depicted in Scheme 1*B*. The heme position is probably slightly different from that in the WT protein, as revealed by rR frequencies that are consistent with differences in the H-bonding environment of the propionates. However, similarity among the other rR features and the HSQC fingerprint for the protein backbone are consistent with the closed protein conformation. We have described a similar situation for the H83A variant in which removal of His^{83} decreases the binding ability of the Tyr and a high spin species is obtained (Scheme 1*C*) (13).

Mutation of His^{32} to Ala creates on the L1 heme side a situation similar to that described above for the L2 side; the long L1 loops assumes its closed conformation (as indicated by HSQC data) thanks to the coordination bond between a water mole-

cule and the iron (Scheme 1*D*). This coordinating H_2O molecule, although in relatively fast exchange with bulk solvent, resides in its coordinating position long enough to give rise to measurable paramagnetic effects on water relaxivity, and therefore, it should give rise to non-negligible, albeit weak, H-bond interactions with L1 residues. Other H-bond interactions involving heme propionates are reasonably still operative. All these factors contribute to shift the equilibrium from the extended conformation of L1 in the apoprotein toward its closed conformation. Some functional considerations can be inferred from the above structural data, as described below.

Functional Implications—The whole body of spectroscopic data offers a unique view of the electronic structure and coordination properties of heme in the two mutants, although the comparison with WT gives insights on the role that the two heme-binding residues, as well as the L1 and L2 loops, play during heme uptake and release processes. When discussed together with x-ray data, available for the HasA complex with its membrane receptor HasR, and molecular dynamics studies of holo- and apo-WT protein, our data offer an innovative picture of conformational equilibria of HasA during heme uptake and release.

Heme Uptake—To date, the mechanism of heme binding to HasA has not been delineated. It has been proposed (9) that formation of the holoprotein occurs via a two-step mechanism where the heme first binds to the pre-formed loop L2, and then the presence of the metal cofactor drives the binding of His^{32} and closure of loop L1. Heme iron binding to His^{32} and formation of the hydrogen bond network on His^{32} side stabilize the L1 loop in its final conformation. The H32A variant characterized here represents a possible intermediate in this mechanism, where the H_2O-bound form may favor the closed conformation of loop L1 according to the following scheme that adds a further step to the previous mechanism

$$\text{apoHasA}_{WT} + \text{heme} \rightarrow (\text{Tyr}^{75}\text{-heme:HasA}_{WT})_{open} \rightarrow (\text{Tyr}^{75}\text{-heme:HasA}_{WT})_{closed} \rightarrow (\text{Tyr}^{75}\text{-heme-His}^{32}\text{:HasA}_{WT})_{closed}$$

SCHEME 2

As in holo-H32A, a water molecule likely occupies the sixth position in the two intermediate His^{32}-off state species and is displaced by His^{32} during the closure of the L1 loop.

Heme Transfer to HasR Receptor—HasA hemophore and HasR form a tight complex, dissociable only after heme has been transferred (45). The x-ray structures of holo-$HasA_{WT}$-HasR and holo-$HasA_{WT}$-HasRI671G, which display a model of the heme-loaded complex before heme transfer, were recently solved (46). However, loop L1 could not be modeled because of missing electron density. On the basis of x-ray data, the following heme transfer mechanism has been proposed. First, two loops of HasR clash with the L1 loop, causing rupture of the axial coordination between His^{32} and heme while coordination between Tyr^{75} and heme persists. Second, displacement of His^{83} induces the breaking of the Tyr^{75}–His^{83} hydrogen bond causing rupture of the Tyr^{75}-heme coordination. Finally, residue Ile^{671} of HasR sterically displaces heme from HasA. This is consistent with the order of axial ligand release predicted from solution rR spectroscopy of WT and mutant HasA-CO complexes (47).

Thus, we propose that the first phase of the holo-$HasA_{WT}$ to HasR docking process is the formation of a closed His^{32}-off state species, similar to H32A. When mapping by NMR the interaction between holo-$HasA_{WT}$ and its receptor (48), we showed that in the holo-$HasA_{WT}$-HasR complex wherein heme had been transferred to HasR, loop L1 has a conformation resembling that of apo-$HasA_{WT}$. Thus, the opening of loop L1 must occur before heme transfer to HasR.

In summary, the already available information for the interaction between HasA and HasR suggests that the heme uptake and release processes may occur via a common intermediate state characterized by a Tyr^{75}-iron bound form with open conformation of loop L1. This state is not accessible to the free protein, even upon substitution of the axial His^{32} ligand with a noncoordinating Ala; we have indeed observed that a water-mediated interaction between iron and L1-loop residues is sufficient to maintain the closed conformation. This finding implies that formation of such an intermediate can only be obtained by the interaction with the partner proteins, which drives the opening of the L1 loop.

Acknowledgments—We thank B. Guigliarelli for EPR data. Bio-NMR Project (Contract 261686) is acknowledged for providing access to NMR and NMRD instrumentations available at Center of Nuclear Magnetic Resonance.

REFERENCES

1. Létoffé, S., Ghigo, J. M., and Wandersman, C. (1994) Iron acquisition from heme and hemoglobin by a *Serratia marcescens* extracellular protein. *Proc. Natl. Acad. Sci. U.S.A.* **91,** 9876–9880
2. Ghigo, J. M., Létoffé, S., and Wandersman, C. (1997) A new type of hemophore-dependent heme acquisition system of *Serratia marcescens* reconstituted in *Escherichia coli*. *J. Bacteriol.* **179,** 3572–3579
3. Létoffé, S., Redeker, V., and Wandersman, C. (1998) Isolation and characterization of an extracellular heme-binding protein from *Pseudomonas aeruginosa* that shares function and sequence similarities with the *Serratia marcescens* HasA hemophore. *Mol. Microbiol.* **28,** 1223–1234
4. Idei, A., Kawai, E., Akatsuka, H., and Omori, K. (1999) Cloning and characterization of the *Pseudomonas fluorescens* ATP-binding cassette exporter, HasDEF, for the heme acquisition protein HasA. *J. Bacteriol.* **181,** 7545–7551
5. Rossi, M. S., Fetherston, J. D., Létoffé, S., Carniel, E., Perry, R. D., and Ghigo, J. M. (2001) Identification and characterization of the hemophore-dependent heme acquisition system of *Yersinia pestis*. *Infect. Immun.* **69,** 6707–6717
6. Izadi, N., Henry, Y., Haladjian, J., Goldberg, M. E., Wandersman, C., Delepierre, M., and Lecroisey, A. (1997) Purification and characterization of an extracellular heme-binding protein, HasA, involved in heme iron acquisition. *Biochemistry* **36,** 7050–7057
7. Arnoux, P., Haser, R., Izadi, N., Lecroisey, A., Delepierre, M., Wandersman, C., and Czjzek, M. (1999) The crystal structure of HasA, a hemophore secreted by *Serratia marcescens*. *Nat. Struct. Biol.* **6,** 516–520
8. Arnoux, P., Haser, R., Izadi-Pruneyre, N., Lecroisey, A., and Czjzek, M. (2000) Functional aspects of the heme-bound hemophore HasA by structural analysis of various crystal forms. *Proteins* **41,** 202–210
9. Wolff, N., Izadi-Pruneyre, N., Couprie, J., Habeck, M., Linge, J., Rieping, W., Wandersman, C., Nilges, M., Delepierre, M., and Lecroisey, A. (2008) Comparative analysis of structural and dynamic properties of the loaded and unloaded hemophore HasA. Functional implications. *J. Mol. Biol.*

376, 517–525
10. Caillet-Saguy, C., Delepierre, M., Lecroisey, A., Bertini, I., Piccioli, M., and Turano, P. (2006) Direct-detected ^{13}C NMR to investigate the iron(III) hemophore HasA. *J. Am. Chem. Soc* **128,** 150–158
11. Deniau, C., Gilli, R., Izadi-Pruneyre, N., Létoffé, S., Delepierre, M., Wandersman, C., Briand, C., and Lecroisey, A. (2003) Thermodynamics of heme binding to the HasA(SM) hemophore. Effect of mutations at three key residues for heme uptake. *Biochemistry* **42,** 10627–10633
12. Wolff, N., Deniau, C., Létoffé, S., Simenel, C., Kumar, V., Stojiljkovic, I., Wandersman, C., Delepierre, M., and Lecroisey, A. (2002) Histidine pK_a shifts and changes of tautomeric states induced by the binding of gallium-protoporphyrin IX in the hemophore HasA(SM). *Protein Sci.* **11,** 757–765
13. Caillet-Saguy, C., Turano, P., Piccioli, M., Lukat-Rodgers, G. S., Czjzek, M., Guigliarelli, B., Izadi-Pruneyre, N., Rodgers, K. R., Delepierre, M., and Lecroisey, A. (2008) Deciphering the structural role of histidine 83 for heme binding in hemophore HasA. *J. Biol. Chem.* **283,** 5960–5970
14. Létoffé, S., Deniau, C., Wolff, N., Dassa, E., Delepelaire, P., Lecroisey, A., and Wandersman, C. (2001) Hemophore-mediated bacterial heme transport. Evidence for a common or overlapping site for heme-free and heme-loaded hemophore on its specific outer membrane receptor. *Mol. Microbiol.* **41,** 439–450
15. Izadi-Pruneyre, N., Wolff, N., Redeker, V., Wandersman, C., Delepierre, M., and Lecroisey, A. (1999) NMR studies of the C-terminal secretion signal of the heme-binding protein, HasA. *Eur. J. Biochem.* **261,** 562–568
16. Dawson, R., Elliott, D., Elliott, W., and Jones, K. (1986) *Data for Biochemical Research*, pp. 233–236, Oxford University Press, Oxford, UK
17. Gsponer, J., Hopearuoho, H., Whittaker, S. B., Spence, G. R., Moore, G. R., Paci, E., Radford, S. E., and Vendruscolo, M. (2006) Determination of an ensemble of structures representing the intermediate state of the bacterial immunity protein Im7. *Proc. Natl. Acad. Sci. U.S.A.* **103,** 99–104
18. Ayed, A., Mulder, F. A., Yi, G. S., Lu, Y., Kay, L. E., and Arrowsmith, C. H. (2001) Latent and active p53 are identical in conformation. *Nat. Struct. Biol.* **8,** 756–760
19. Bruschi, M., Bertrand, P., More, C., Leroy, G., Bonicel, J., Haladjian, J., Chottard, G., Pollock, W. B., and Voordouw, G. (1992) Biochemical and spectroscopic characterization of the high molecular weight cytochrome *c* from *Desulfovibrio vulgaris* Hildenborough expressed in *Desulfovibrio desulfuricans* G200. *Biochemistry* **31,** 3281–3288
20. Evans, D. F. (1959) 400. The determination of the paramagnetic susceptibility of substances in solution by nuclear magnetic resonance. *J. Chem. Soc.* 2003–2005
21. Phillips, W. D., and Poe, M. (1972) Contact shifts and magnetic susceptibilities in iron-sulfur proteins as determined from nuclear magnetic resonance spectra. *Methods Enzymol.* **24,** 304–317
22. Bertini, I., Luchinat, C., Turano, P., Battaini, G., and Casella, L. (2003) The magnetic properties of myoglobin as studied by NMR spectroscopy. *Chemistry* **9,** 2316–2322
23. Bertini, I., Luchinat, C., and Parigi, G. (2001) *Solution NMR of Paramagnetic Molecules*, Elsevier, Amsterdam
24. Deniau, C., Couprie, J., Simenel, C., Kumar, V., Stojiljkovic, I., Wandersman, C., Delepierre, M., and Lecroisey, A. (2001) ^{1}H, ^{15}N, and ^{13}C resonance assignments for the gallium protoporphyrin IX-HasA(sm) hemophore complex. *J. Biomol. NMR* **21,** 189–190
25. Streit, B. R., Blanc, B., Lukat-Rodgers, G. S., Rodgers, K. R., and DuBois, J. L. (2010) How active-site protonation state influences the reactivity and ligation of the heme in chlorite dismutase. *J. Am. Chem. Soc.* **132,** 5711–5724
26. Chakrabarti, P. (1990) Geometry of interaction of metal ions with histidine residues in protein structures. *Protein Eng.* **4,** 57–63
27. Bertini, I., Luchinat, C., Parigi, G., and Walker, F. A. (1999) Heme methyl ^{1}H chemical shifts as structural parameters in some low spin ferriheme proteins. *J. Biol. Inorg. Chem.* **4,** 515–519
28. Jin, Y., Nagai, M., Nagai, Y., Nagatomo, S., and Kitagawa, T. (2004) Heme structures of five variants of hemoglobin M probed by resonance Raman spectroscopy. *Biochemistry* **43,** 8517–8527
29. Hu, S., and Kincaid, J. R. (1992) Resonance Raman studies of the carbon-monoxy form of catalase. Evidence for and effects of phenolate ligation. *FEBS Lett.* **314,** 293–296
30. Eakanunkul, S., Lukat-Rodgers, G. S., Sumithran, S., Ghosh, A., Rodgers, K. R., Dawson, J. H., and Wilks, A. (2005) Characterization of the periplasmic heme-binding protein shut from the heme uptake system of *Shigella dysenteriae*. *Biochemistry* **44,** 13179–13191
31. Stevens, J. M., Uchida, T., Daltrop, O., Kitagawa, T., and Ferguson, S. J. (2006) Dynamic ligation properties of the *Escherichia coli* heme chaperone CcmE to noncovalently bound heme. *J. Biol. Chem.* **281,** 6144–6151
32. Sun, J., Loehr, T. M., Wilks, A., and Ortiz de Montellano, P. R. (1994) Identification of histidine 25 as the heme ligand in human liver heme oxygenase. *Biochemistry* **33,** 13734–13740
33. Franzen, S., Bailey, J., Dyer, R. B., Woodruff, W. H., Hu, R. B., Thomas, M. R., and Boxer, S. G. (2001) A photolysis-triggered heme ligand switch in H93G myoglobin. *Biochemistry* **40,** 5299–5305
34. Hu, S., Smith, K. M., and Spiro, T. G. (1996) Assignment of Protoheme resonance Raman spectrum by heme labeling in myoglobin. *J. Am. Chem. Soc.* **118,** 12638–12646
35. Smulevich, G., Hu, S., Rodgers, K. R., Goodin, D. B., Smith, K. M., and Spiro, T. G. (1998) Heme-protein interactions in cytochrome *c* peroxidase revealed by site-directed mutagenesis and resonance Raman spectra of isotopically labeled hemes. *Biospectroscopy* **2,** 365–376
36. Heering, H. A., Jansen, M. A., Thorneley, R. N., and Smulevich, G. (2001) Cationic ascorbate peroxidase isoenzyme II from tea. Structural insights into the heme pocket of a unique hybrid peroxidase. *Biochemistry* **40,** 10360–10370
37. Siebel, J. F., Kosinsky, R. L., Åkerström, B., and Knipp, M. (2012) Insertion of heme *b* into the structure of the Cys^{34}-carbamidomethylated human lipocalin α_1-microglobulin. Formation of a $[(heme)_2\ (\alpha_1\text{-microglobulin})]_3$ complex. *ChemBioChem* **13,** 879–887
38. Ikezaki, A., and Nakamura, M. (2002) Models for cytochromes *c*′. Spin states of mono(imidazole)-ligated (meso-tetramesitylporphyrinato)iron(III) complexes as studied by UV-Vis, ^{13}C NMR, ^{1}H NMR, and EPR spectroscopy. *Inorg. Chem.* **41,** 6225–6236
39. Bondon, A., and Mouro, C. (1998) PASE (paramagnetic signals enhancement). A new method for NMR study of paramagnetic proteins. *J. Magn. Reson.* **134,** 154–157
40. Hildebrand, D. P., Burk, D. L., Maurus, R., Ferrer, J. C., Brayer, G. D., and Mauk, A. G. (1995) The proximal ligand variant H93Y of horse heart myoglobin. *Biochemistry* **34,** 1997–2005
41. Zeng, Y., Caignan, G. A., Bunce, R. A., Rodríguez, J. C., Wilks, A., and Rivera, M. (2005) Azide-inhibited bacterial heme oxygenases exhibit an S = 3/2 (*dxz,dyz*)3(*dxy*)1(*dz*2)1 spin state. Mechanistic implications for heme oxidation. *J. Am. Chem. Soc.* **127,** 9794–9807
42. Aime, S., Fasano, M., Paoletti, S., Cutruzzolà, F., Desideri, A., Bolognesi, M., Rizzi, M., and Ascenzi, P. (1996) Structural determinants of fluoride and formate binding to hemoglobin and myoglobin. Crystallographic and ^{1}H NMR relaxometric study. *Biophys. J.* **70,** 482–488
43. Motie, M., Kassner, R. J., Meyer, T. E., and Cusanovich, M. A. (1990) Kinetics of cyanide binding to *Chromatium vinosum* ferricytochrome *c*′. *Biochemistry* **29,** 1932–1936
44. Bertini, I., and Turano, P. (2007) in *Biological Inorganic Chemistry* (Bertini, I., Gray, H. B., Stiefel, E. I., and Valentine, J. S., eds) 1st Ed, pp. 31–56, University Science Books, Sausalito, CA
45. Izadi-Pruneyre, N., Huché, F., Lukat-Rodgers, G. S., Lecroisey, A., Gilli, R., Rodgers, K. R., Wandersman, C., and Delepelaire, P. (2006) The heme transfer from the soluble HasA hemophore to its membrane-bound receptor HasR is driven by protein-protein interaction from a high to a lower affinity binding site. *J. Biol. Chem.* **281,** 25541–25550
46. Krieg, S., Huché, F., Diederichs, K., Izadi-Pruneyre, N., Lecroisey, A., Wandersman, C., Delepelaire, P., and Welte, W. (2009) Heme uptake across the outer membrane as revealed by crystal structures of the receptor-hemophore complex. *Proc. Natl. Acad. Sci. U.S.A.* **106,** 1045–1050
47. Lukat-Rodgers, G. S., Rodgers, K. R., Caillet-Saguy, C., Izadi-Pruneyre, N., and Lecroisey, A. (2008) Novel heme ligand displacement by CO in the soluble hemophore HasA and its proximal ligand mutants. Implications for heme uptake and release. *Biochemistry* **47,** 2087–2098
48. Caillet-Saguy, C., Piccioli, M., Turano, P., Izadi-Pruneyre, N., Delepierre, M., Bertini, I., and Lecroisey, A. (2009) Mapping the interaction between the hemophore HasA and its outer membrane receptor HasR using CRINEPT-TROSY NMR spectroscopy. *J. Am. Chem. Soc* **131,** 1736–1744